

Green and facile synthesis of sponge-reinforced silica aerogel and its pumping application for oil absorption

Song He¹ · Xudong Cheng¹ · Zhi Li¹ · Xiaojing Shi¹ · Hui Yang¹ · Heping Zhang¹

Received: 3 July 2015 / Accepted: 8 September 2015 / Published online: 1 December 2015
© Springer Science+Business Media New York 2015

Abstract In this paper, we have prepared methyltrimethoxysilane (MTMS)-based sponge-reinforced silica aerogel with low density through facile synthesis within 12 h. The sample's mechanical property has been improved significantly compared with pure MTMS-based silica aerogel. The aerogels are hydrophobic and oleophilic. And its absorption capacity to the organic liquids is excellent. To overcome the low efficiency of traditional desorption methods (squeezing or distilling), the obtained sample is inserted by a stainless steel pipe which is connected to a pump. The novel design can realize the aerogels' continuous absorption ability. The pumping rate is significantly affected by the aerogels' pore size and the organic liquids' viscosity, which is consistent with the simple proposed model in this paper. Such an apparatus means that a small piece of this sponge-reinforced silica aerogel can continuously collect a large area of floating oil from a water surface with high speed and efficiency.

Introduction

Water contaminations caused by oils or organic solvents can severely threaten the people and environment [1]. To control the accidental and unconscious release of oil/organic liquids effectively, a wide range of oil remediation materials have been employed as absorbents [2], dispersants [3], and so on. Among them, the hydrophobic porous

materials are commonly used due to their excellent features such as low density and high porosity [4]. The hydrophobic aerogels, such as the polyvinyl alcohol-cellulose nanofibril hybrid aerogels (PACNHA) [1], the methyltriethoxysilane (MTES)-based aerogels [5], spongy graphene [6], and functional hydrophobic sponge [7, 8] have all shown excellent absorption capacity to oils. However, most of these studies focused excessively on the oil sorption capacity (amount of oil absorbed per unit weight/volume of sorbent), but ignored the high material and transport costs of these light-weight sorbent materials, especially in pelagic environment. Moreover, fossil fuels are nonrenewable sources; thus, the recovery of oil from absorbents is necessary. Although the absorber oils can be desorbed from the absorbents by squeezing [9] and distillation [6], the time-consuming and poor efficient procedures are obstacles for their practical and commercial application. Although the absorption capacity of some porous absorbents is extremely high, like spongy graphene (more than 80 times of their own weight [6]), their continuous adsorption ability should be improved further if applied to actual and large scale absorption of spilled organics. The pumping method [10] gives a perfect solution, although some pores within the hydrophobic SiO₂-coated polymer sponge are caulked which is inevitable in the preparation process. On the other hand, the preparation cost of these porous materials is usually very expensive and the preparation process is relatively complex and time consuming.

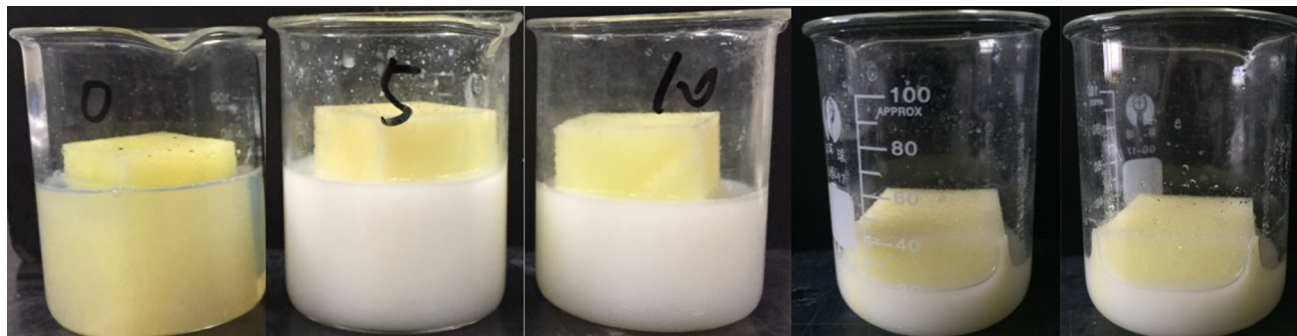
Previously, we have synthesized sponge-reinforced monolithic silica aerogels using Tetraethyl orthosilicate (TEOS) as precursor [11]. And the aerogels show excellent absorption capacity of organics. However, the compressive stress is relatively high, so it is hard to separate the absorbed oils from the aerogels other than drying. In addition, the preparation process is relatively complex,

✉ Heping Zhang
zhanghp@ustc.edu.cn

¹ State Key Laboratory of Fire Science, University of Science and Technology of China, Hefei 230027, Anhui, People's Republic of China

Table 1 Raw material composition and density of PUS-reinforced aerogel samples

Sample	MTMS (ml)	EtOH (ml)	H ₂ O (ml)	CTAB (g)	Bulk density (g/cm ³)	Si density (g/cm ³)
S-1	5	0	15	0.1	0.585 (±4 %)	0.183 (±4 %)
S-2	5	2.5	12.5	0.1	0.405 (±3 %)	0.127 (±3 %)
S-3	5	5	10	0.1	0.141 (±2 %)	0.045 (±2 %)
S-4	5	10	10	0.1	0.126 (±2 %)	0.038 (±2 %)
S-5	5	15	10	0.1	0.114 (±2 %)	0.034 (±2 %)

**Fig. 1** Photographs of wet gels S1, S2, S3, S4, and S5 (left to right)

including aging, solvent exchanging, and surface modification. In this research, a more facile and green method is presented and a new material is made. Instead of TEOS, we chose MTMS as the precursor. Properly utilizing phase separation could control the pores distribution within the gels [12]. For the fact that the compressive strength of pure MTMS-based silica aerogel is relatively low [13], polyurethane sponge (PUS) is used as the reinforcement material. And the compressive stress of the as-prepared aerogel has been significantly improved compared to either pure silica aerogel or PUS. The entire preparation process can be finished within 12 h under ambient pressure, which is much shorter than the previous studies [5, 14]. Without extra surface modification, the hydrophobicity and lipophilicity of the as-prepared aerogel are excellent. Most importantly, the absorbed organic liquids within the pores can be pumped out successively, and the product can be recycled for many times.

Materials and methods

Sample preparation

MTMS is chosen as precursor. Other agents, including *n*-hexadecyltrimethylammonium bromide (CTAB) as cationic surfactant, ammonium hydroxide (NH₄OH) as base catalyst, hydrochloric acid (HCl) as acid catalyst, ethanol (EtOH) and deionized water (DI·H₂O) as the solvents, were purchased from Sinopharm Chemical Reagent Co., Ltd. The PUS was purchased from 3M Company.

HCl and NH₄OH were diluted with deionized water (DI·H₂O) to 0.1 and 0.5 M, respectively. The PUS was cleaned ultrasonically with acetone and distilled water successively to remove possible impurities. Then, they were dried under 100 °C for 2 h. In a typical synthesis, 5 ml MTMS, 1000 μl 0.1 M HCl, and 0.1 g CTAB were mixed in a 100 ml beaker. Mixed solvent (EtOH and DI·H₂O) was subsequently added to the beaker. The mixture was stirred vigorously. Then, 10 mol/l aqueous NH₄OH aqueous solution was added to modify the pH of the solution to ~8 after 20 min. Thereafter, refined PUS with appropriate dimension was put into the sol. The gelation occurred within 3 h. Then, the gel was dried in ambient pressure at 100 °C for 8 h to get the samples. The starting compositions and properties of aerogels are presented in Table 1.

Characterization

Compression test was conducted using an Instron (E3000K8953) (250 N load, 0.5 mm/min) in which the sample size is 10-mm long, 10-mm wide, and 20-mm high. The microstructure of the aerogels was studied using a FESEM (SIRION 200, FEI, USA). FTIR spectra were obtained using Nicolet 8700 (Thermo Fisher Scientific, USA). And the XPS tests were conducted by Thermo ESCALAB 250 (Thermo-VG Scientific, USA). The obtained samples with a size of 30 mm × 30 mm × 30 mm were immersed into mixtures prepared using various types of solvents/oils and water with a 1:1 volume ratio [1]. The absorption process was fast and generally reached

equilibrium within a few minutes. Then, the soaked samples were taken out and weighed after the aerogel surface was swiped using a filter paper to remove extra surface solvent/oil [15]. The absorptivity (Q) was determined using Eq. (1)

$$Q(\%) = \frac{(W - W_0) - (m_0 - m)}{\rho_L V_0} \times 100\%, \quad (1)$$

where W_0 and W are the weights of aerogels, respectively, before and after absorption; m_0 and m are the weights of water before and after absorption. V_0 is the aerogel volume and ρ_L is the density of absorbed solvent/oil. The data acquisition system includes a PC and a SHIMADZU electronic balance (UW6200H, Japan).

Results and discussion

Pore structure

Surfactant was introduced to MTMS-based system to obtain continuous and nanoscale porous structure [16]. The surfactant can suppress the macroscopic phase separation during gelation [12]. In our research, CTAB is chosen as the surfactant. In the system without any EtOH (sample S1), phase separation is prohibited by the surfactant, and the condensation reaction among SiO_2 oligomers is suppressed. Continuous and nanoporous structure is formed, and the wet gel is translucent [16]. As to the samples S2, S3, S4, and S5, the formed gels suffer opacification. With the increasing of EtOH, the macroscopic phase separation enhances. The monomers and oligomers are concentrated in one of the phases after the onset of phase separation, which can more effectively undergo condensation with nearer neighboring species [12]. Then, macropores formed and the gels become more and more opaque, as shown in Fig. 1. The addition of EtOH weakens the surfactant's suppression effect of phase separation. The pore sizes of wet gel become larger with the increasing of EtOH.

When dried under ambient pressure, capillary pressure occurs and forces to the pores. The capillary pressure of a fluid in a pore is a function of the pore fluid/vapor surface tension, \mathcal{T} , the contact angle that the fluid/vapor interface makes with the pore wall, θ , and a characteristic capillary size, r , which is related to the pore size, r_p . Assuming that the pores are cylindrical, the magnitude of the capillary pressure (P) in a single pore is given as [17]

$$p = 2\mathcal{T}\cos\theta/r_p \quad (2)$$

And most investigators assume that $r = r_p$ [17, 18]. Evidently, capillary pressure forced to small pore is stronger than that of the ones exerted on large pores. On the other hand, pores with small diameter have a weaker

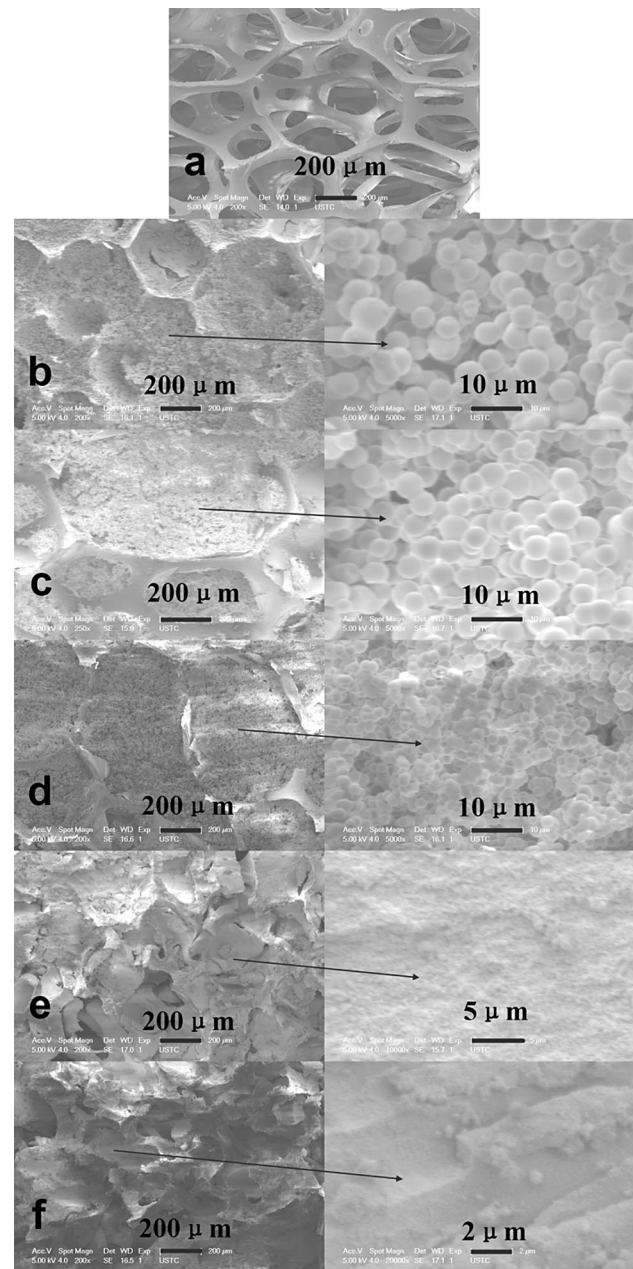


Fig. 2 SEM images of **a** sponge, **b** S5, **c** S4, **d** S3, **e** S2, **f** S1

resistance to withstand the capillary pressure compared with pores of large size. Thus, when dried under ambient pressure, nanopores within S1 and S2 collapsed and the aerogels shrank heavily. No evident pores can be seen in the SEM images (Fig. 2e, f). As a result, the PUS pores are destroyed seriously as shown in Fig. 2e and f. While the macropores in S3, S4, and S5 rarely collapsed, so continuous and porous 3D structure can be obtained (Fig. 2b, c and d).

The samples (including PUS, PUS-reinforced silica aerogel (S5), and pure MTMS-based silica aerogel) were characterized by X-ray photoelectron spectroscopy (XPS),

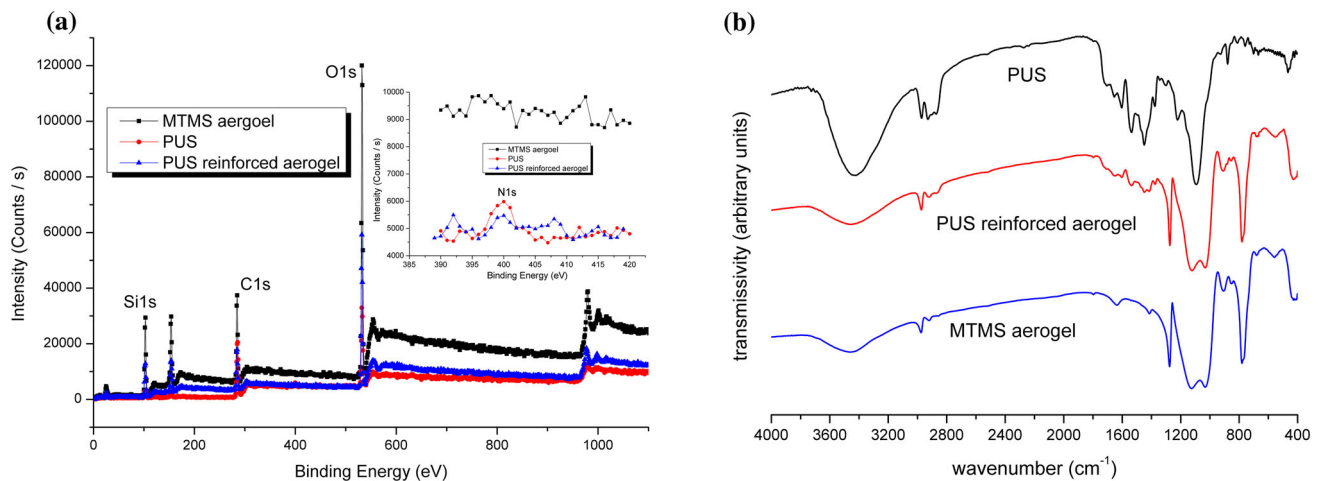


Fig. 3 XPS (a) and FTIR (b) spectra of the samples (including PUS, PUS-reinforced silica aerogel, and pure MTMS-based silica aerogel)

as shown in Fig. 3a. The main peak at 283.3 eV is due to C 1 s of carbon atoms, 531.3 eV is due to O 1 s of oxygenate atoms, 103.1 eV attributes to Si 1 s of silica atoms, and 400.0 eV is due to N 1 s of nitrogen atoms. The N 1 s band is obtained from PUS. The FTIR spectra are presented in Fig. 3b. It can be seen that compared with spectra of PUS and MTMS-based aerogel, there is no evident new absorption peak in the PUS-reinforced silica aerogel. The spectra of PUS-reinforced aerogel can be simply seen as the spectral combination result of PUS and MTMS-based aerogel. As a result, there is no evident new chemical bond generated between the aerogel particles and PUS during the preparation process.

Mechanical properties

For the sample S1, the nanopores collapsed when dried under ambient pressure, so there are almost no continuous pores within S1 after drying. As to the samples S4 and S5, the macropores rarely collapsed during drying, so continuous and macroporous structure can be obtained which results in excellent elasticity of the aerogels [5, 13]. Figure 4a shows the compression–depression process of S5.

The samples S3, S4, and S5 experienced two deformation stages when compressed (shown in Fig. 4b): elastic deformation and plastic deformation. In the first stage, the sponge-reinforced silica aerogel experienced the reversible shrinkage. When releasing the stress, the aerogel can return to its original status, and the structure of the samples remains the same as the original ones. The stress can reach to 140 kPa when the strain is 50 %, which is much stronger than the methyltrichlorosilane-modified PUS [8] (~13.5 kPa at 50 % strain). According to Kazuyoshi et al. [16], three factors help to promote the elastic deformation. The fact that only three siloxane bonds per each silicon

atom lowers the crosslinking density and makes the macroscopic gel more flexible than pure silica aerogels (TEOS-based silica aerogels, for example). Second, low density of silanol groups hinders the nonreversible shrinkage. And finally, methyl groups are homogeneously distributed with high density in the network, which will repel each other during the temporal shrinkage on compression. After the elastic deformation, with the further increase of strain, the compressive stress just changed a little. In this stage, the porous structure of silica aerogels within the sponge pores may be destroyed and cannot withstand the stress further, although the sample can almost return to its original shape when releasing stress. For sample with lower density, the porosity is higher; thus, there is more space to be compressed before mechanical failure. So, with the lowest density, the compressive strain of S5 is the largest before the plastic deformation. It can be seen in Fig. 2 that pore distribution of S5 is the most uniform one of the three (S3, S4, and S5); thus, when compressed, the load forced on the every single pore is almost the same. For less uniform pore structure, the load forced on the pore is not uniform, so it is easy to be deformed. As a result, for less uniform pore structure, the stress is weaker at the same strain compared with the ones with uniform pore structure. As to the samples S1 and S2, there is almost no pore within the microstructure, so evident elastic and plastic deformation in the curve cannot be seen (Fig. 4c). Compared with S2, particles within S1 display in a more closed way. So, the stress forced on S1 at the same stain is stronger than that forced on S2.

Adsorption capacity

For the existence of methyl (–CH₃) groups, the MTMS-based silica aerogels are hydrophobic and oleophilic

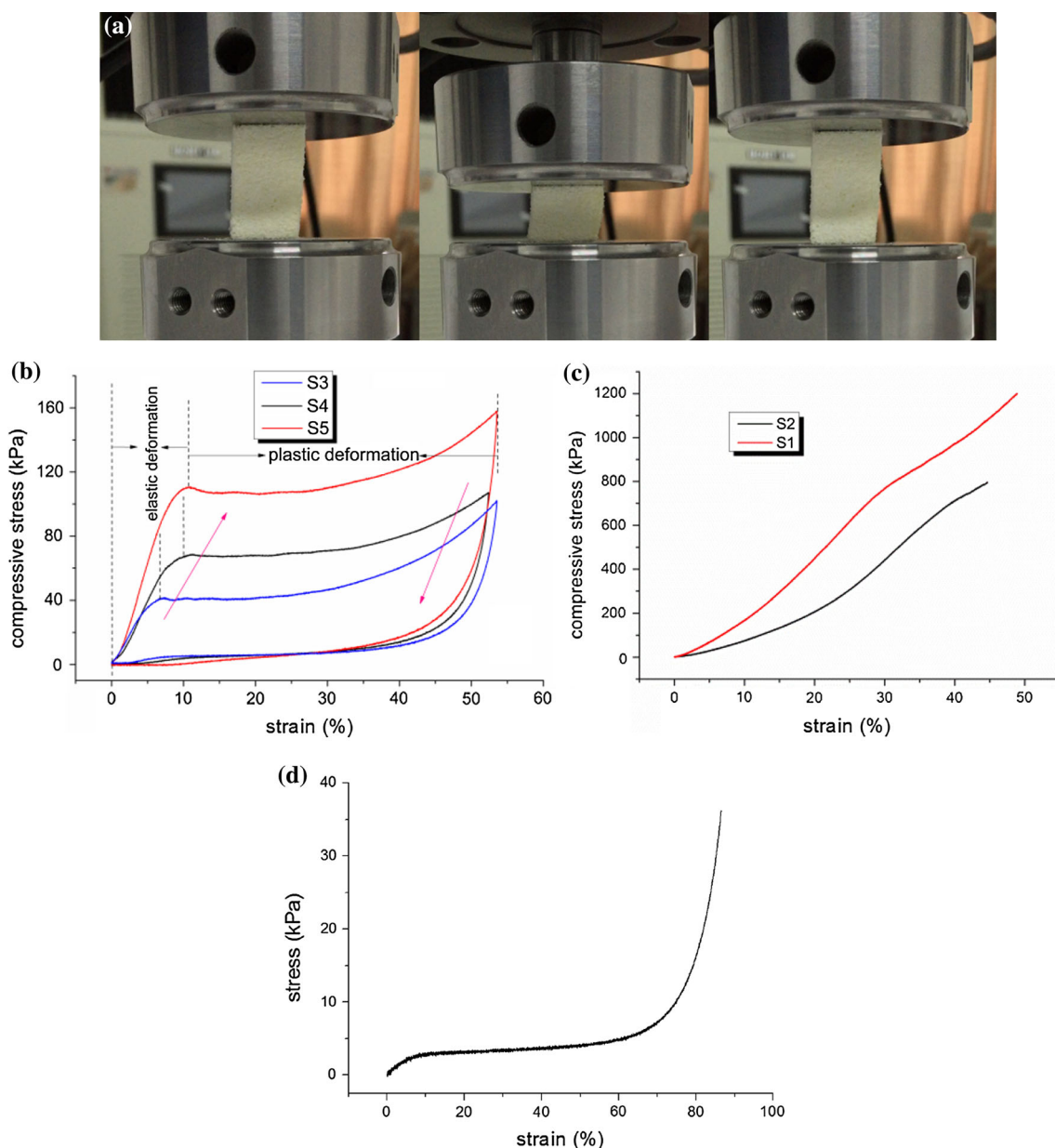


Fig. 4 **a** Compression–depression test of S5, compressive strain–stress curve of PUS-reinforced aerogel samples, **b** S3, S4, and S5, **c** S1 and S2, **d** PUS

which can be clearly illustrated in Fig. 5a and Movie S1. And the aerogel can remain excellent hydrophobicity after adsorption (Fig. 5a). A water droplet can stay at the surface of the sponge-reinforced silica aerogel, whereas *n*-hexane droplets will be completely absorbed immediately once contacted to the aerogel surface. The adsorption process usually takes <2 s. Figure 5b and Movie S2 present a series process the sponge-reinforced silica aerogels absorb *n*-hexane floating on the water. The aerogel absolutely absorbed the *n*-hexane within seconds. The aerogel filled with *n*-hexane could be left floating on the water without any oil release or water absorption. In

addition, the aerogel can resist acid, alkali, and salt solution well, which can be seen in Fig. 5c. The adsorption capacity to various organic liquids of the as-prepared sponge-reinforced silica aerogels is measured and presented in Fig. 6. More than 0.7 ml organic liquid can be absorbed by 1 cm³ aerogels. Figure 6 also compares the absorption capacity of different porous materials, which indicates excellent adsorption capacity of the as-prepared sponge-reinforced silica aerogel. The volume normalized absorption capacity in the soot dipped PUS exceeds 1 ml/cm³ may be caused by the volume expansion after adsorption of the liquids.

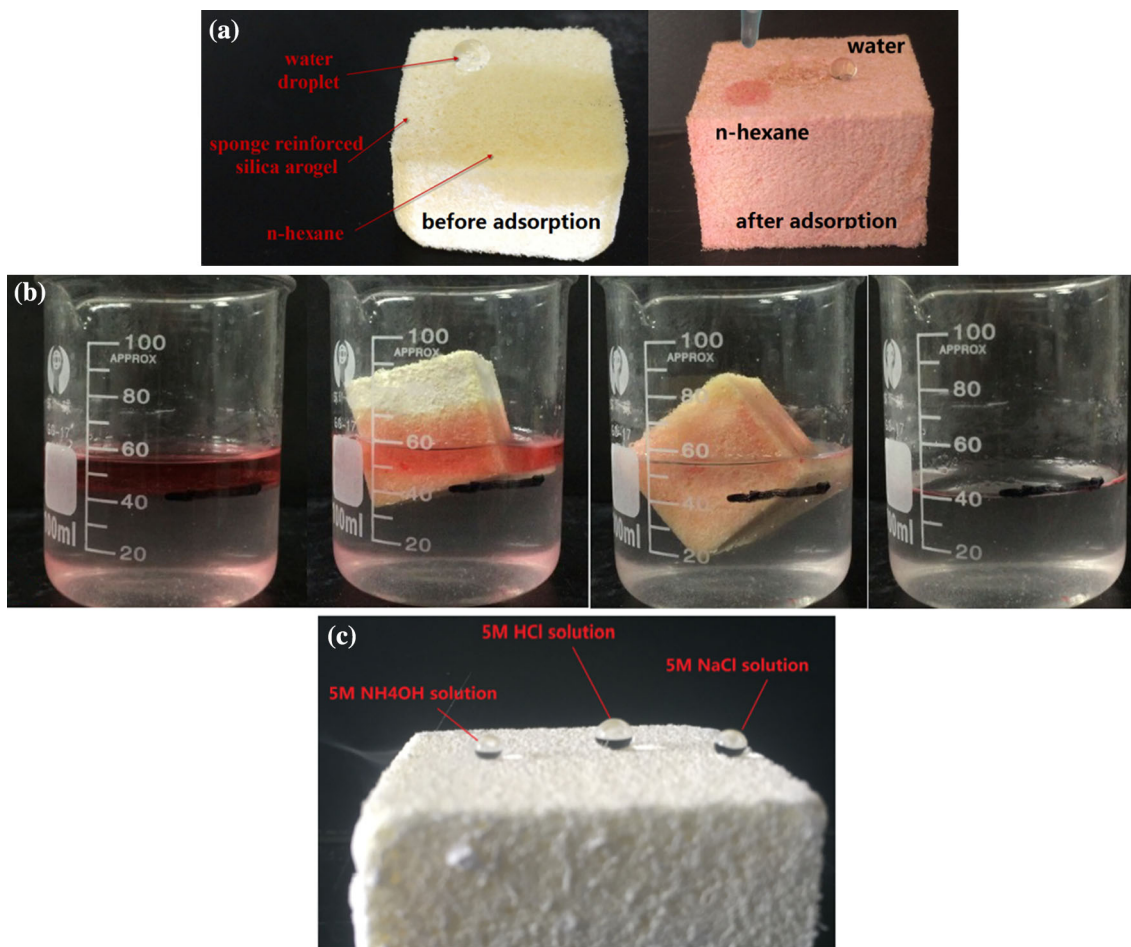


Fig. 5 a *n*-Hexane and water droplet dropped on surface of sponge-reinforced silica aerogel before and after adsorption (after 10 adsorption–desorption cycles). b Sponge-reinforced silica aerogel

absorb *n*-hexane (labeled by *Oil Red O*) floating on the water. c Salt, acid, and alkali solution dropped on the aerogel surface (Color figure online)

Pumping mechanism

Although with excellent absorption capacity to organic liquids, the desorption process and the collection of the absorbed liquids could be hard for the as-prepared sponge-reinforced silica aerogels. To solve this problem, a thin pipe (thickness: 0.2 mm, diameter: 10.0 mm, Fig. 7a) connecting a pump is inserted into the sponge-reinforced silica aerogel, as shown in Fig. 7b. The whole pumping system is presented in Fig. 7c. Before implying suction force, the capillary pressure at oil–air and oil–water interfaces can be regulated by decreasing or increasing the curvature radius of corresponding interface to reach equilibrium with the pressure at the nozzle of pipe [10] (Fig. 8a). When suction force is applied, the equilibrium is broken, and the oil above the nozzle of the pipe was pumped further away (Fig. 8b) until no oil is above the nozzle. Then, air channels form, leaving behind the oil that was below the nozzle of the pipe (Fig. 8c). In this way, the

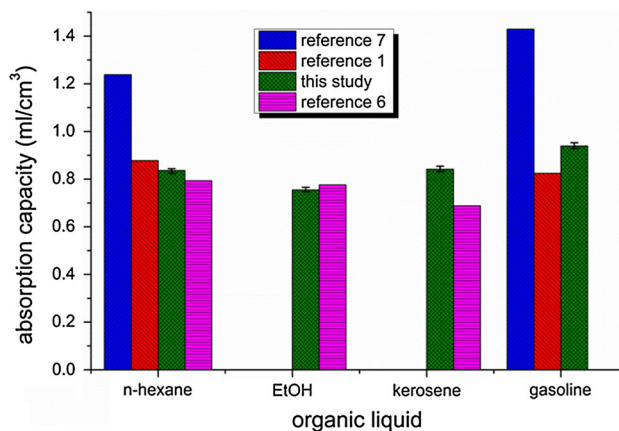


Fig. 6 Comparison of adsorption capacities of different materials

as-prepared sponge-reinforced silica aerogel connecting a pumping device can continuously absorb and collect oils floating on the water, indicating a much more efficient way

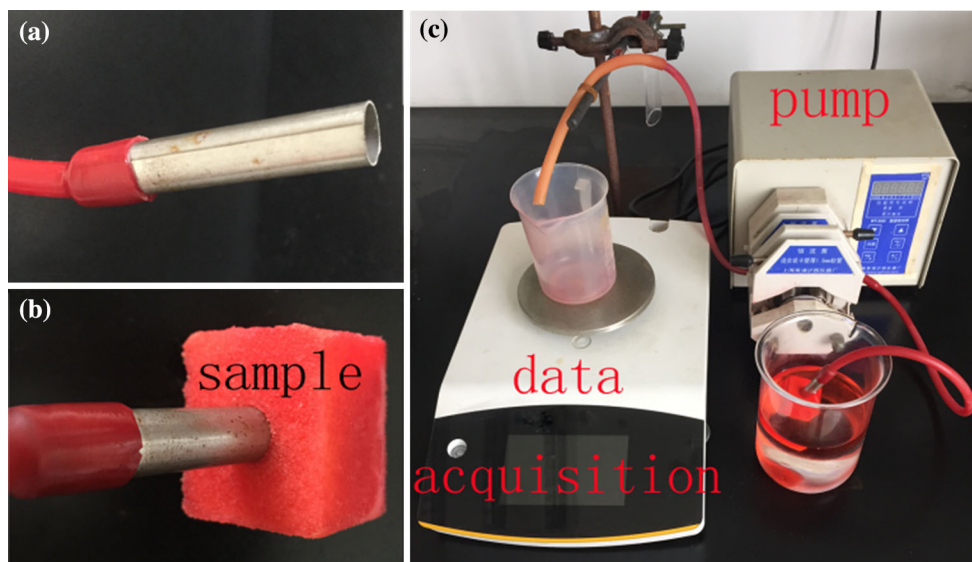


Fig. 7 Pumping facility **a** stainless steel pipe, **b** sample inserted by the steel pipe, **c** whole system

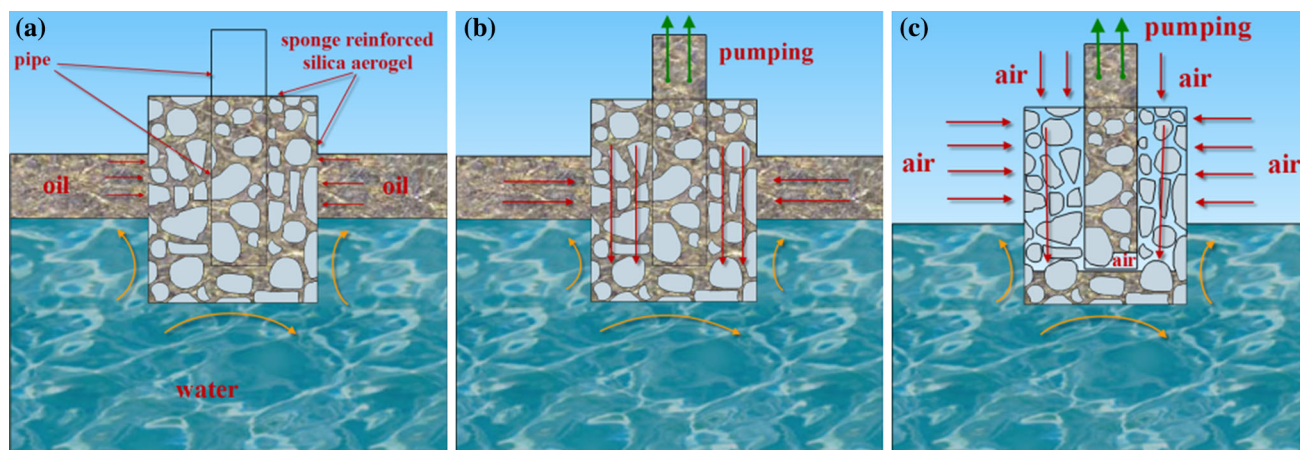


Fig. 8 Schematic diagram of pumping process

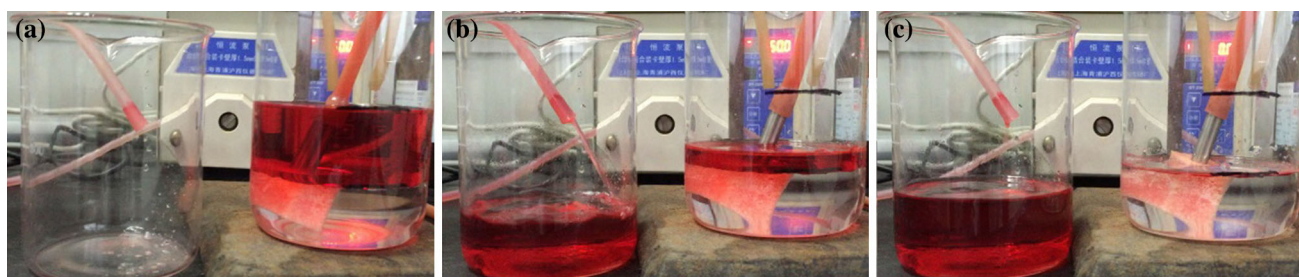


Fig. 9 *n*-Hexane floating on water (labeled with *Oil Red O*) pumped by S5. **a** Initial stage of pumping, **b** during pumping, **c** ending of pumping (Color figure online)

to collecting oils than squeezing [9] and distillation [6]. In a verification experiment, the sample S5 was used to absorb *n*-hexane (labeled with *Oil Red O*) floating on water. The upper surface of the sample was not in contact with *n*-

hexane. And *n*-hexane was pumped out quickly (see in Movie S3). Extremely, in another experiment, the sample was intentionally pressed down to contact with water, leaving a small part in the *n*-hexane section (Fig. 9a). For

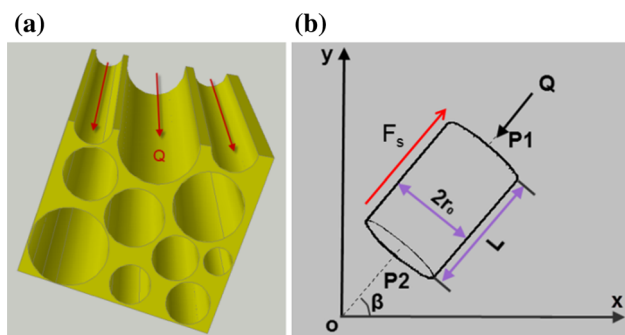


Fig. 10 **a** Schematic diagram of capillaries in aerogels, **b** stress diagram of liquids in capillaries

the pressure offered by the pump, *n*-hexane was continuously absorbed by the sample and pumped out (Fig. 9b, c). No water was collected (Fig. 9c). The detailed pumping process can be seen in Movie S4. We can see that even in case of roaring waves, as long as the part of sample contacts with the oil, this apparatus can collect oil from water efficiently.

To better understand the pumping mechanism of the liquids within the pores of open-porous materials, a simple model has been developed. For the open pore structure, liquids flow through the pores to the destination. It is hard to accurately calculate the flow rate directly. It can be assumed that the pores within the silica aerogels comprise a number of ordered capillaries as shown in Fig. 10a. Then, organic liquids flow through these capillaries under pressure. The stress diagram of liquid within the capillary is shown in Fig. 10b. Friction exerting on the fluid within the capillary can be expressed as follows:

$$F_s = 2\pi rL\tau \tag{3}$$

where τ is shearing stress, according to law of Newton inner friction:

$$\tau = -\mu \frac{du}{dr} \tag{4}$$

μ is the dynamical viscosity of the fluid. When the fluid within the capillary is in a balanced state, in which the fluid is going to move when the pressure increases or decreases just a little.

$$F_p + F_G = F_s \tag{5}$$

$$(P1 - P2)\pi r^2 + \rho\pi r^2 Lg \sin \beta = \pm 2\pi rL\tau \tag{6}$$

$$\tau = \pm \frac{r(P1 - P2 + \rho gL \sin \beta)}{2L} \tag{7}$$

$$u = \mp \frac{P1 - P2 + \rho gL \sin \beta}{4\mu L} (r_0^2 - r^2) \tag{8}$$

The mass flux of the fluid can be obtained as

$$Q = 2\pi \int_0^{r_0} ur dr = \mp \pi \frac{P1 - P2 + \rho gL \sin \beta}{8\mu L} r_0^4 \tag{9}$$

$Q \propto \mu^{-1}$, increasing the fluid’s dynamical viscosity will lead to the drop of mass flux. $Q \propto r^4$, so the mass flux of the fluid pumping out is largely affected by the average pore diameter. If the pore is too small, it is hard to pump out the liquids within the pores even if a high pressure is applied to the surface. To verify, several pumping experiments were conducted.

To investigate the influence of liquid viscosity, several organic liquids of different dynamic viscosities were chosen to test the pumping rate, such as *n*-hexane (0.3 mPa s), kerosene (2.7 mPa s), dimethyl silicone oil 1 (10 mPa s), dimethyl silicone oil 2 (20 mPa s), and dimethyl silicone oil 3 (50 mPa s). Before applying a suction force, the sample was put into the organic liquid to reach the absorption saturation state. The maximum speed of the pump is 150 r/min. The pumping curve of S5 is presented in Fig. 11a. It took about 80 s to collect ~58 ml *n*-hexane. However, the collection time gets longer as the liquid’s dynamic viscosity increases. The pumping rate almost remained the same during the whole experiments. Through linear fitting, we can get the pumping rate, which would decrease when rising the liquid’s viscosity, as shown in Fig. 11b. The higher pump speed means larger value of P1–P2. As a result, the pumping rate will increase with the rising of pump speed. The experiment results are consistent with the Eq. (9).

Pore sizes significantly affect the pumping rate. Samples with various pore sizes were tested to pump *n*-hexane, including our previously synthesized mesoporous TEOS-based sponge-reinforced silica aerogel [11]. The results can be seen in Fig. 11c, in which the pumping rate significantly varies with pore sizes. The samples with structure of mesopores (TEOS-based PUS-reinforced silica aerogel) or even smaller pores (S1) cannot pump any *n*-hexane at all, although the viscosity of *n*-hexane is the lowest of the four. For pores of nanoscale or even smaller, pressure forced on the pore is weaker compared with that of larger pores under the same pressure (P1–P2). Theoretically, increasing the pressure may pump out the liquids within the small pores, but before which, the high pressure may destroy the sample structure (Fig. 11d). The pumping rate gradually increases with the rise of pore size. The pumping rate of materials with pores of hundreds of micrometers has been studied already [10] which is even larger. Figure 11e gives the pumping rate at speed of 150 r/min. For the samples S1 and S2, their pores are too small for the organic liquids to go through and no liquid can be pumped out. As to the other samples, the pumping rate increases with the rising of the

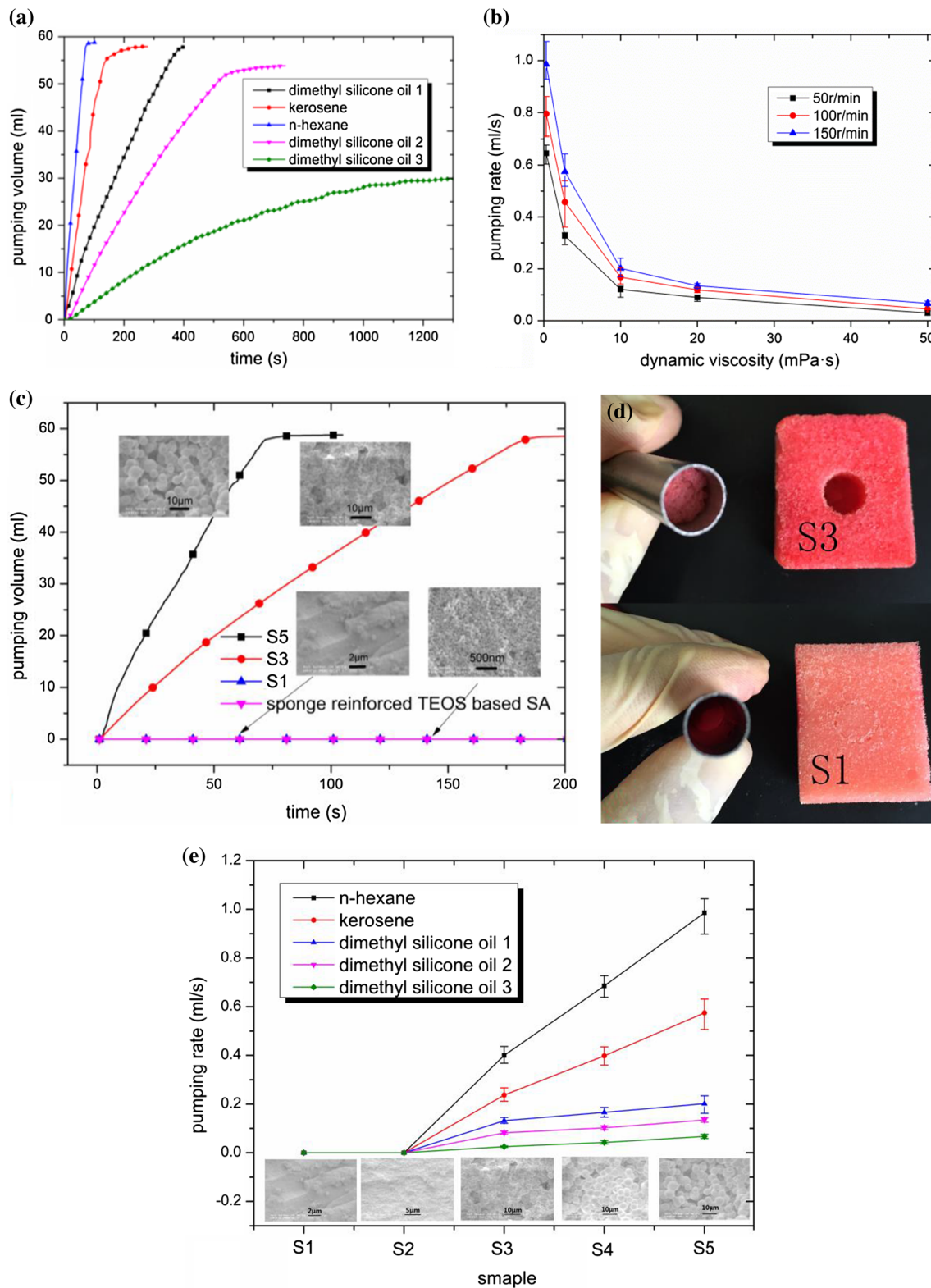


Fig. 11 **a** Pumping curve of S5 at 100 r/min, **b** pumping rate of S5 to different organic liquids, **c** *n*-hexane pumping curve of samples with different pore sizes at 100 r/min, **d** sample and steel pump after

pumping dimethyl silicone oil 3, **e** pumping rate of the samples at speed of 150 r/min

pore sizes. And the pumping rate will decrease if the liquid's viscosity gets larger.

This adsorption system, which can continuously absorb oil from water with high efficiency, avoids carrying lots of adsorption materials and can save much space especially in pelagic environment. As a result, considerable amount of transport cost can be saved.

Conclusion

MTMS-based PUS-reinforced silica aerogel with low density has been prepared through facile and green synthesis within 12 h. The sample's mechanical property has been improved significantly compared with pure MTMS-based silica aerogel. The aerogels are hydrophobic and oleophilic. The adsorption capacity to the organic liquids is excellent, and more than 0.7 ml organic liquid can be absorbed by 1 cm³ PUS-reinforced silica aerogel. To realize the aerogels' continuous absorption ability, the aerogel is inserted by a stainless steel pipe which is connected to a pump. The pumping rate is significantly affected by the aerogels' pore size and liquids' viscosity, which is consistent with the model we developed. Pore size is a restriction to the pumping rate. Increasing the average pore size will speed up the fluid flow within the capillaries. On the contrary, rising the viscosity of the liquid would increase the friction between the capillaries and the fluids. As a result, the pumping rate will decrease. To verify, several experiments were conducted and the results were consistent with model we developed. Such an apparatus means that a small piece of this PUS-reinforced silica aerogel can continuously collect a large area of floating oil from a water surface with high speed and efficiency.

Acknowledgements This work was supported by the National Basic Research Program of China (973 Program) (2012CB719701) and Fundamental Research Funds for the Central Universities (WK2320000032).

References

- Zheng Q, Cai Z, Gong S (2014) Green synthesis of polyvinyl alcohol (PVA)–cellulose nanofibril (CNF) hybrid aerogels and their use as superabsorbents. *J Mater Chem A* 2:3110–3118
- Liang H-W, Guan Q-F, Chen L-F et al (2012) Macroscopic-scale template synthesis of robust carbonaceous nanofiber hydrogels and aerogels and their applications. *Angew Chem Int Ed* 51:5101–5105
- Kujawinski EB, Kido Soule MC, Valentine DL et al (2011) Fate of dispersants associated with the deepwater horizon oil spill. *Environ Sci Technol* 45:1298–1306
- Toyoda M, Inagaki M (2000) Heavy oil sorption using exfoliated graphite: new application of exfoliated graphite to protect heavy oil pollution. *Carbon* 38:199–210
- Yu YX, Wu XY, Guo DQ et al (2014) Preparation of flexible, hydrophobic, and oleophilic silica aerogels based on a methyltriethoxysilane precursor. *J Mater Sci* 49:7715–7722. doi:10.1007/s10853-014-8480-0
- Bi H, Xie X, Yin K et al (2012) Spongy graphene as a highly efficient and recyclable sorbent for oils and organic solvents. *Adv Funct Mater* 22:4421–4425
- Xi P, Huang L, Xu Z et al (2014) Low cost and robust soot dipped polyurethane sponge for highly efficient and recyclable oil and organic solvent cleanup. *RSC Adv* 4:59481–59485
- Zhu Q, Chu Y, Wang Z et al (2013) Robust superhydrophobic polyurethane sponge as a highly reusable oil-absorption material. *J Mater Chem A* 1:5386–5393
- Nguyen DD, Tai N-H, Lee S-B et al (2012) Superhydrophobic and superoleophilic properties of graphene-based sponges fabricated using a facile dip coating method. *Energy Environ Sci* 5:7908–7912
- Ge J, Ye Y-D, Yao H-B et al (2014) Pumping through porous hydrophobic/oleophilic materials: an alternative technology for oil spill remediation. *Angew Chem Int Ed* 53:3612–3616
- He S, Cheng X, Li Z et al (2015) Facile synthesis of sponge reinforced monolithic silica aerogels with improved mechanical property and excellent absorptivity. *Mater Lett* 154:107–111
- Kanamori K, Nakanishi K (2011) Controlled pore formation in organotrialkoxysilane-derived hybrids: from aerogels to hierarchically porous monoliths. *Chem Soc Rev* 40:754–770
- Xu B, Cai JY, Xie Z et al (2012) An improved method for preparing monolithic aerogels based on methyltrimethoxysilane at ambient pressure part II: microstructure and performance of the aerogels. *Microporous Mesoporous Mater* 148:152–158
- Xu B, Cai JY, Finn N et al (2012) An improved method for preparing monolithic aerogels based on methyltrimethoxysilane at ambient pressure part I: process development and macrostructures of the aerogels. *Microporous Mesoporous Mater* 148:145–151
- Wu T, Chen M, Zhang L et al (2013) Three-dimensional graphene-based aerogels prepared by a self-assembly process and its excellent catalytic and absorbing performance. *J Mater Chem A* 1:7612–7621
- Kanamori K, Aizawa M, Nakanishi K et al (2008) Elastic organic–inorganic hybrid aerogels and xerogels. *JSGST* 48:172–181
- Smith DM, Scherer GW, Anderson JM (1995) Shrinkage during drying of silica gel. *J Non-Cryst Solids* 188:191–206
- Jeffrey Brinker C, Scherer GW (1990) *Sol-gel science: the physics and chemistry of sol-gel processing*. Academic Press, San Diego